

DeepSolo++: Let Transformer Decoder with Explicit Points Solo for Text Spotting

Maoyuan Ye, Jing Zhang, *Senior Member, IEEE*, Shanshan Zhao, Juhua Liu, Tongliang Liu, *Senior Member, IEEE*, Bo Du, *Senior Member, IEEE*, Dacheng Tao, *Fellow, IEEE*

Abstract—End-to-end text spotting aims to integrate scene text detection and recognition into a unified framework. Dealing with the relationship between the two sub-tasks plays a pivotal role in designing effective spotters. Although Transformer-based methods eliminate the heuristic post-processing, they still suffer from the synergy issue between the sub-tasks and low training efficiency. In this paper, we present **DeepSolo**, a simple DETR-like baseline that lets a single **Decoder** with **Explicit Points Solo** for text detection and recognition simultaneously and efficiently. Technically, for each text instance, we represent the character sequence as ordered points and model them with learnable explicit point queries. After passing a single decoder, the point queries have encoded requisite text semantics and locations, thus can be further decoded to the center line, boundary, script, and confidence of text via very simple prediction heads in parallel. Furthermore, we show the surprisingly good extensibility of our method, in terms of character class, language type, and task. On the one hand, DeepSolo not only performs well in English scenes but also masters the Chinese transcription with complex font structure and a thousand-level character classes. On the other hand, based on the extensibility of DeepSolo, we launch **DeepSolo++** for multilingual text spotting, making a further step to let Transformer decoder with explicit points solo for multilingual text detection, recognition, and script identification all at once. Extensive experiments on public benchmarks demonstrate that our simple approach achieves better training efficiency compared with Transformer-based models and outperforms the previous state-of-the-art. For example, on ICDAR 2019 ReCTS for Chinese text, DeepSolo boosts the 1-NED metric to a new record of 78.3%. On ICDAR 2019 MLT, DeepSolo++ achieves absolute 5.5% H-mean and 8.0% AP improvements on joint detection and script identification task, and 2.7% H-mean gains on end-to-end spotting. In addition, DeepSolo and DeepSolo++ are also compatible with line annotations, which require much less annotation cost than polygons. The code is available at <https://github.com/VITAE-Transformer/DeepSolo>.

Index Terms—Text spotting, DETR, Explicit point query, Multilingual

1 INTRODUCTION

Detecting and recognizing text in natural scenes, *a.k.a.* text spotting, has drawn increasing attention due to its wide range of applications [1], [2], such as intelligent navigation [3]. How to deal with the relationship between detection and recognition is a long-standing and open problem, which has a significant impact on structural pipeline, performance, efficiency, annotation cost, *etc.*

Most pioneering end-to-end spotting methods focus on one specific language scene, especially English, without launching a unified model for several languages. The majority of them [4], [5], [6], [7], [8], [9], [10] follow a detect-

then-recognize pipeline, which first detects text instances and then exploits crafted Region-of-Interest (RoI) operation to extract features within the detected area, finally feeds them into a following recognizer (Fig. 1(c)). Although these methods have achieved great progress, there are two main limitations. 1) The extra RoI transform for feature alignment is indispensable. Some RoI operations require polygon annotations, which are not applicable when only weak annotations (*e.g.*, lines) are available. 2) Additional efforts are desired to address the synergy issue between the detection and recognition modules [11], [12]. In contrast, segmentation-based methods [13], [14] try to isolate the two sub-tasks and conduct spotting in a parallel multi-task framework with a shared backbone (Fig. 1(b)). Nevertheless, they are sensitive to noise and require grouping post-processing to gather unstructured components.

Beyond monolingual text spotting, when it comes to multilingual text spotting, existing methods [15], [16], [17], [18] still lie in the detect-then-recognize flow. In addition, to solve the script identification task introduced in the multilingual scenarios and allow for more convenient customization of recognizers for different languages, Huang *et al.* [17], [18] devise tailored language predictors and use them for routing to a recognizer. Despite the novel framework, the overall pipeline undergoes unfortunate expansion, growing in complexity with the added modules (Fig. 1(d)). Extra efforts are involved in designing a language predictor with appropriate structure and exploring a module-wise multi-stage training pipeline.

This work was supported in part by the National Natural Science Foundation of China under Grants 62076186 and 62225113, and in part by the Science and Technology Major Project of Hubei Province (Next-Generation AI Technologies) under Grant 2019AEA170. Dr. Jing Zhang was supported by Australian Research Council Projects in part by FL170100117 and IH180100002. The numerical calculations in this paper have been done on the supercomputing system in the Supercomputing Center of Wuhan University. Maoyuan Ye and Jing Zhang contributed equally to this work. Corresponding authors: Juhua Liu, Bo Du (e-mail: {liujuhua, dubo}@whu.edu.cn). M. Ye and J. Liu are with the Research Center for Graphic Communication, Printing and Packaging, Institute of Artificial Intelligence, Wuhan University, China (e-mail: {yemaoyuan, liujuhua}@whu.edu.cn). B. Du is with the National Engineering Research Center for Multimedia Software, Institute of Artificial Intelligence, School of Computer Science and Hubei Key Laboratory of Multimedia and Network Communication Engineering, Wuhan University, China (e-mail: dubo@whu.edu.cn). J. Zhang, T. Liu, and D. Tao are with the School of Computer Science, Faculty of Engineering, The University of Sydney, Australia (email: {jing.zhang1, tongliang.liu}@sydney.edu.au; dacheng.tao@gmail.com). S. Zhao is with the JD Explore Academy at JD.com, China (email: sshan.zhao00@gmail.com).

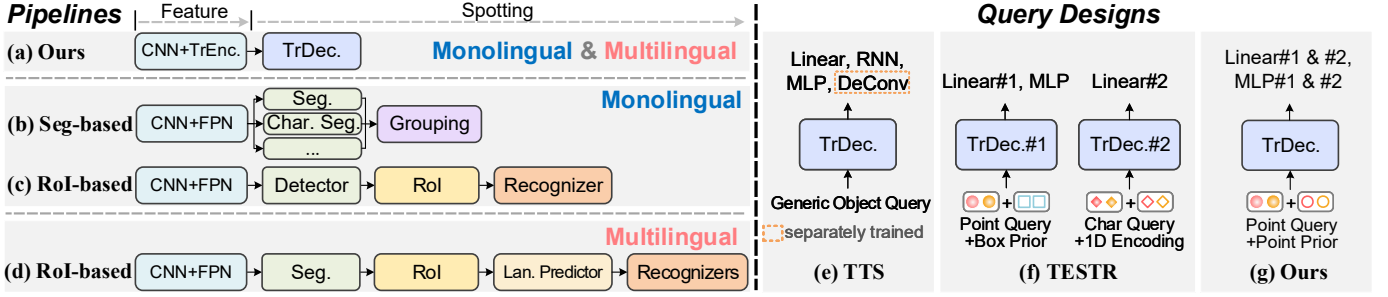


Fig. 1 – Comparison of text spotting pipelines and query designs. In our method, for both monolingual and multilingual text spotting, the spotting part is a solo by the Transformer decoder with explicit points. ‘TrEnc.’ (‘TrDec.’): Transformer encoder (decoder). ‘Char.’: characters. ‘Seg.’: segmentation. ‘Lan. Predictor’: language prediction network.

In recent years, Transformer [19] has shown eminent flexibility and sparked the performance remarkably for various computer vision tasks [20], [21], [22], including text spotting [12], [23], [24], [25]. Although the text spotters [23], [25] based on DETR [26] can get rid of RoI and heuristic post-processing, they lack efficient and joint representation to deal with scene text detection and recognition, *e.g.*, requiring an extra RNN module in TTS [25] (Fig. 1(e)) or exploiting individual Transformer decoder for each sub-task in TESTR [23] (Fig. 1(f)). The generic object query exploited in TTS fails to consider the unique characteristics of scene text, *e.g.*, location and shape. While TESTR adopts point queries with box positional prior that is coarse for point predicting, and the queries are different between detection and recognition, introducing unexpected heterogeneity. Consequently, these designs hamper the performance and training efficiency [27]. Last but not least, the potential of Transformer on multilingual text spotting is unexplored.

In this paper, we propose a novel query form based on explicit point representations of text lines. Built upon it, we present a succinct DETR-like baseline that lets a single **Decoder with Explicit Points Solo** (dubbed **DeepSolo**) for detection and recognition simultaneously. Moreover, we launch a simple multilingual text spotter (dubbed **DeepSolo++**), making a further step to let a single decoder solo for detection, recognition, and script identification all at once (Fig. 1(a) and Fig. 1(g)). Technically, for each instance, we first represent the character sequence as ordered points, where each point has explicit attributes of position, offsets to the top and bottom boundary, and category. Specifically, we devise top- K Bezier center curves to fit scene text instances with arbitrary shapes and sample a fixed number of on-curve points covering characters in each text instance. Then, we leverage the sampled points to generate positional queries and guide the learnable content queries with explicit positional prior. After flowing out the decoder, the output queries are expected to have encoded requisite text semantics and locations. Finally, we adopt several simple prediction heads (a linear layer or MLP) in parallel to decode the queries into the center line, boundary, transcript, and confidence of text, thereby solving detection and recognition simultaneously. For multilingual spotting, we introduce an extra explicit point query as the script token and use it for script identification and routing to a specific linear layer for character classification. We also devise a simple script-aware matching scheme for the training of DeepSolo++.

In summary, the main contributions are four-fold:

- We propose a novel query form based on explicit points sampled from the Bezier center curve representation of text instance lines, which can efficiently encode the position, shape, and semantics of text, thus helping simplify both the monolingual and multilingual text spotting pipeline.
- We propose succinct yet effective baseline models named DeepSolo and DeepSolo++ for monolingual and multilingual text spotting, respectively.
- Our method shows several good properties, including 1) **simplicity** of model structure and training pipeline, 2) **efficiency** of training and inference, and 3) **extensibility** of character class, language, and task.
- Extensive experiments on challenging datasets demonstrate the state-of-the-art (SOTA) performance of our method and some other distinctions, such as the effectiveness on dense and long text, and the flexibility of position annotation form.

The rest of this paper is organized as follows. In Sec. 2, we briefly review the related works. In Sec. 3, we introduce our proposed DeepSolo and DeepSolo++, in detail. Sec. 4 and Sec. 5 report our experimental results for DeepSolo and DeepSolo++, respectively, and is followed by a discussion in Sec. 6. Finally, we conclude our study in Sec. 7.

2 RELATED WORKS

2.1 RoI-based Text Spotters

Taking the merit of joint optimization of both detection and recognition networks, recent works dive into developing end-to-end text spotters. Most of them craft RoI [28] or Thin-Plate Splines (TPS) [29] to bridge detector and recognizer. In [4], [30], given the detection results, RoIAlign or its variants are exploited to extract text features for the following recognizer. Mask TextSpotter series [8], [9], [31] conduct character segmentation for recognition based on the RoIAligned features. GLASS [10] devises a plug-in global-to-local attention module to enhance the representation ability with the assistance of Rotated-RoIAlign. In comparison, [32], [33] use TPS to rectify curve texts with control points. To better rectify curved texts, ABCNet series [5], [6] propose the BezierAlign module using parameterized Bezier curve. Although these methods successfully bridge scene text detection and recognition serially, they ignore the synergy issue [11], [12] between the two tasks. To overcome this dilemma, SwinTextSpotter [12] proposes a

tailored Recognition Conversion module to back-propagate recognition information to the detector. Although the above methods have achieved remarkable progress, they require an extra RoI-based or TPS-based module. Since some RoI operations require polygon annotations, the methods may be not applicable to scenarios with only weak position annotations (e.g., single points, lines). Moreover, a more effective and simpler solution is also expected to address the synergy issue.

2.2 RoI-free Text Spotters

To get rid of the extra RoI transform, [13], [14] adopt parallel dense heads to segment characters and instances. They achieve promising throughput but rely on heuristic grouping as post-processing.

Inspired by DETR family [26], [34], recent works [23], [24], [25] explore the Transformer framework without RoIAlign and complicated post-processing. TESTR [23] adopts two parallel Transformer decoders for detection and recognition. TTS [25] adds an RNN recognizer into Deformable-DETR [34] and shows its potential on weak annotations. Differently, from the perspective of sequence prediction paradigm, SPTS [24] demonstrates that using single-point or even script-only annotations is feasible and promising. Although these methods unlock the potential of Transformer in text spotting, there are still some limitations. For example, the vanilla or individual queries used in TTS and TESTR cannot efficiently encode text features (e.g., location, shape, and semantics), affecting the training efficiency [27] and even increasing the model complexity. Besides, the axis-aligned box annotations used in TTS might not be ideal enough [24] for scene text since the box contains a certain portion of background regions and even other texts, thus introducing extra noise. In our work, thanks to the proposed novel explicit query form, text detection and recognition tasks enjoy an efficient and unified pivot. Moreover, DeepSolo is also compatible with weak text position annotation form, i.e., text center line, which is less affected by background and other instances.

2.3 Multilingual Text Spotting

The majority of existing works focus on training one model using data from a specific language. However, they did not unveil the capability of identifying script and recognizing text instances varying from multiple languages in a single unified network. Only a few works investigated end-to-end multilingual text spotters and achieved exciting results. Among them, E2E-MLT [15] proposes a framework for multilingual text spotting by handling characters from all languages in the same recognizer, the same as CRAFTS [16]. In comparison, Multiplexed TextSpotter [17] and Grouped TextSpotter [18] leverage several adapted recognizers to deal with different languages respectively, with Language Prediction Network (LPN) routing the detected text to an appropriate recognizer. However, all of the above methods rely on RoI and sequence-to-sequence recognizers. Besides, in [17], [18], hand-crafted LPNs are required for script identification and multi-head routing. From a different paradigm, we demonstrate that our simple baseline, i.e., DeepSolo++ with a simple routing scheme for multilingual recognition,

can reach higher performance without a RoI operation, neither with a specific language prediction network nor adapted recognizers.

2.4 Comparison to the Conference Version

A preliminary version of this paper was previously introduced in [35]. Building upon it, our current study expands significantly, incorporating three major improvements.

- 1) We investigate the performance of DeepSolo on Chinese scene text, characterized by more complex font structures and a larger character set compared to English. DeepSolo delivers SOTA 1-NED result on ICDAR 2019 ReCTS [36], outperforming previous SOTA [37] which leverages language modeling Transformer recognizer. It demonstrates the inherent simplicity and remarkable extensibility of DeepSolo in tackling challenging language scenes.
- 2) We extend DeepSolo to a new baseline model dubbed DeepSolo++ for multilingual text spotting. It simplifies the multilingual text spotting pipeline (Fig. 1(a) vs. Fig. 1(d)) and achieves better performance with a simpler training pipeline on ICDAR 2019 MLT [38] and ICDAR 2017 MLT [39]. It validates the extensibility of our method on a new task.
- 3) Additional experiment results, encompassing the effectiveness of DeepSolo on dense and long scene text, its robustness in handling highly rotated instances, and other relevant factors, are presented. Moreover, comprehensive ablation studies, in-depth analyses, and supplementary visualization results are provided to augment the research findings.

3 DEEPSOLO

In this paper, we propose **DeepSolo** for text spotting. DeepSolo aims to efficiently detect and recognize text simultaneously with a single Transformer decoder by digging into the close relationship between text detection and recognition. Building upon DeepSolo, we extend it to **DeepSolo++** for multilingual text spotting, which retains structural simplicity by leveraging the single decoder to solo for multilingual detection, recognition, and script identification.

3.1 Overview

Preliminary. Bezier curve, firstly introduced into text spotting by ABCNet [5], can flexibly fit the shape of scene text with a certain number of control points. Different from ABCNet which crops features with BezierAlign, we explore the distinctive utilization of the Bezier curve in the DETR framework. More details of the Bezier curve generation can be referred to [5], [6]. Given four Bezier control points¹ for each side (top and bottom) of a text instance, we simply compute Bezier control points for the center curve by averaging the corresponding control points on the top and bottom sides. Then, a fixed number of N points are uniformly sampled on the center, top, and bottom curves,

1. Provided by ABCNet [5]

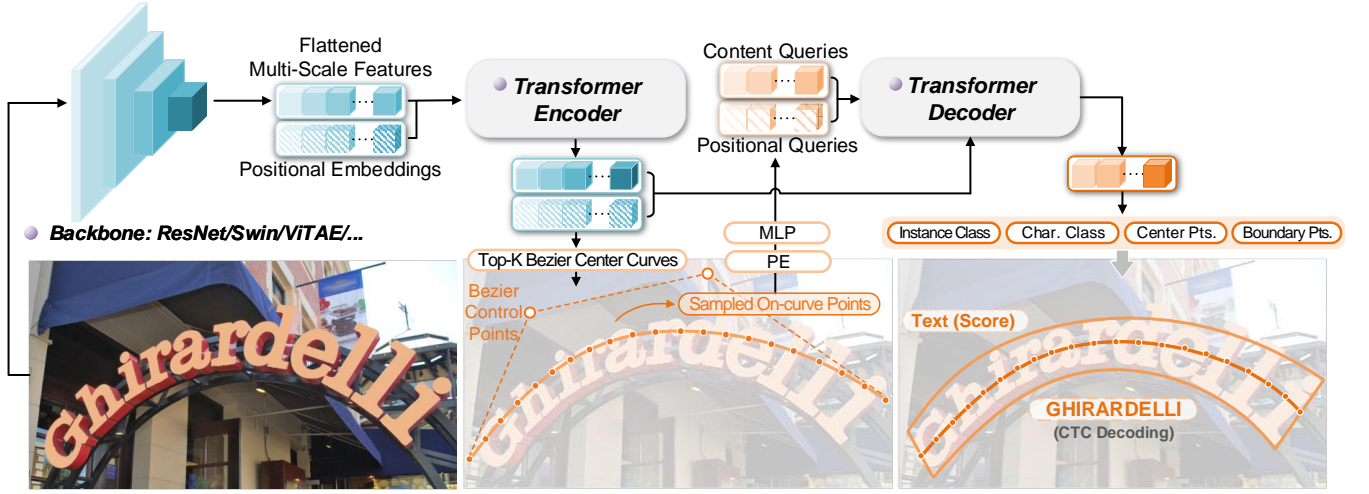


Fig. 2 – The architecture of DeepSolo. We propose an explicit query form based on the points sampled from the Bezier center curve representation of text, solving spotting with a single decoder and simple prediction heads in a unified and concise framework.

serving as the ground truth. Note that the order of on-curve points should be in line with the text reading order.

Model Architecture. The overall architecture is depicted in Fig. 2. After receiving the image features from the encoder equipped with deformable attention [34], Bezier center curve proposal represented by four Bezier control points and the corresponding score are generated. Then, the top- K scored proposals are selected. For each selected curve proposal, N points are uniformly sampled on the curve. The coordinates of these points are encoded as positional queries and added to learnable content queries, forming composite queries. Next, the composite queries are fed into the decoder to gather useful text features via deformable cross-attention. Following the decoder, four simple parallel heads are adopted, each of which is responsible for solving a specific task.

3.2 Top- K Bezier Center Curve Proposals

Different from the box proposal adopted in previous works [23], [27], [34], which has the drawbacks in representing text with arbitrary shape, we design a simple Bezier center curve proposal scheme from the text center line perspective. It can efficiently fit scene text and distinguish one from others, which also makes the usage of line annotations possible. Specifically, given the image features from the encoder, on each pixel of the feature maps, a 3-layer MLP (8-dim in the last layer) is used to predict offsets to four Bezier control points, determining a curve that represents one text instance. Let i index a pixel from features at level $l \in \{1, 2, 3, 4\}$ with 2D normalized coordinates $\hat{p}_i = (\hat{p}_{ix}, \hat{p}_{iy}) \in [0, 1]^2$, its corresponding Bezier control points $BP_i = \{\bar{b}p_{i0}, \bar{b}p_{i1}, \bar{b}p_{i2}, \bar{b}p_{i3}\}$ are predicted:

$$\bar{b}p_{ij} = (\sigma(\Delta p_{ix_j} + \sigma^{-1}(\hat{p}_{ix})), \sigma(\Delta p_{iy_j} + \sigma^{-1}(\hat{p}_{iy}))), \quad (1)$$

where $j \in \{0, 1, 2, 3\}$, σ is the sigmoid function. MLP head only predicts the offsets $\Delta p_{i\{x_0, y_0, \dots, x_3, y_3\}}$. Moreover, we use a linear layer for text or not text classification. And top- K scored curves are selected as proposals.

3.3 Point Query Modeling for Text Spotting

Query Initialization. Given the top- K proposals $\hat{BP}_k (k \in \{0, 1, \dots, K-1\})$, we uniformly sample N points on each curve according to the Bernstein Polynomials [40]. Here, we get normalized point coordinates $Coords$ of shape $K \times N \times 2$ in each image. The point positional queries \mathbf{P}_q of shape $K \times N \times 256$ are generated by:

$$\mathbf{P}_q = \text{MLP}(\text{PE}(\text{Coords})), \quad (2)$$

where PE represents the sinusoidal positional encoding function. Following [41], we also adopt a 2-layer MLP head with ReLU activation for further projection. On the other side, we initialize point content queries \mathbf{C}_q using learnable embeddings. Then, we add \mathbf{P}_q to \mathbf{C}_q to get the composite queries \mathbf{Q}_q :

$$\mathbf{Q}_q = \mathbf{C}_q + \mathbf{P}_q. \quad (3)$$

We empirically exploit unshared point embeddings for \mathbf{C}_q , i.e., N point content queries of shape $N \times 256$ in one text instance are used for each of the K proposals.

Query Update in the Decoder. After obtaining the composite queries \mathbf{Q}_q , we feed them into the Transformer decoder. We follow previous works [23], [27], [42] to first mine the relationship between queries within one text instance using an intra-group self-attention across dimension N . Here, keys are the same with queries while values only contain the content part: $\mathbf{K}_q = \mathbf{Q}_q$, $\mathbf{V}_q = \mathbf{C}_q$. Then, an inter-group self-attention is conducted across K instances to capture the relationship between different instances. The updated composite queries are further sent into the deformable cross-attention to aggregate multi-scale text features from the encoder. The point coordinates $Coords$ are used as the reference points in the deformable attention.

With the explicit point information flowing in the decoder, we adopt a 3-layer MLP head to predict the offsets and update point coordinates after each decoder layer. Then, the updated coordinates will be transformed into new positional queries by Eq. (2).

3.4 Parallel Prediction

After getting queries of shape $K \times N \times 256$ from the decoder for each image, we adopt simple prediction heads to solve

following sub-tasks. **(1) Instance classification.** We use a linear projection for binary classification (text or background). During inference, we take the mean of N scores as the confidence score for each instance. **(2) Character classification.** As the points are uniformly sampled on the center curve of each text instance to cover characters, each point query represents a specific class (including background). We adopt a linear projection to perform character classification. **(3) Center curve points.** Given the explicit point coordinates $Coords$, a 3-layer MLP head MLP_{coord} is used to predict the coordinate offsets from reference points to ground truth points on the center curve. **(4) Boundary points.** Similarly, a 3-layer MLP head MLP_{bd} is used to predict the offsets to the ground truth points on the top and bottom curves.

3.5 Optimization

Bipartite Matching. After obtaining the prediction set \hat{Y} and the ground truth (GT) set Y , similar to [23], we use the Hungarian algorithm [43] to get an injective function $\varphi : [Y] \mapsto [\hat{Y}]$ that minimizes the matching cost \mathcal{C} :

$$\arg \min_{\varphi} \sum_{g=0}^{G-1} \mathcal{C}(Y^{(g)}, \hat{Y}^{(\varphi(g))}), \quad (4)$$

where G is the number of GT instances per image.

Regarding the cost \mathcal{C} , previous work [23] only considers the class and position similarity while ignoring the similarity of the text script. However, matched pairs with similar positions may be quite different in texts, which could increase the optimization difficulty. TTS [25] proposes a cross-entropy-based text matching criterion to address this issue, but it is not applicable to our method since the character predictions are not aligned with the ground truth due to background class and repeated characters. We introduce a text matching criterion based on the typical Connectionist Temporal Classification (CTC) loss [44] which copes with the length inconsistency issue. For the g -th GT and its matched query, the complete cost function is:

$$\begin{aligned} \mathcal{C}(Y^{(g)}, \hat{Y}^{(\varphi(g))}) = & \lambda_{cls} \text{FL}'(\hat{b}^{(\varphi(g))}) + \lambda_{text} \text{CTC}(t^{(g)}, \hat{t}^{(\varphi(g))}) \\ & + \lambda_{coord} \sum_{n=0}^{N-1} \|p_n^{(g)} - \hat{p}_n^{(\varphi(g))}\|, \end{aligned} \quad (5)$$

where λ_{cls} , λ_{text} , and λ_{coord} are hyper-parameters to balance different tasks. $\hat{b}^{(\varphi(g))}$ is the probability for the text-only instance class. The same as [23], FL' is defined as the difference between the positive and negative term: $\text{FL}'(x) = -\alpha(1-x)^{\gamma} \log(x) + (1-\alpha)x^{\gamma} \log(1-x)$, which is derived from the focal loss [45]. The second term is the CTC loss between the GT text $t^{(g)}$ and prediction $\hat{t}^{(\varphi(g))}$. The third term is the L1 distance between the GT $p_n^{(g)}$ and predicted point coordinates $\hat{p}_n^{(\varphi(g))}$ on the center curve.

Overall Loss. For the k -th query, the focal loss for instance classification is formulated as:

$$\begin{aligned} \mathcal{L}_{cls}^{(k)} = & -\mathbb{1}_{\{k \in \text{Im}(\varphi)\}} \alpha(1 - \hat{b}^{(k)})^{\gamma} \log(\hat{b}^{(k)}) \\ & - \mathbb{1}_{\{k \notin \text{Im}(\varphi)\}} (1 - \alpha)(\hat{b}^{(k)})^{\gamma} \log(1 - \hat{b}^{(k)}), \end{aligned} \quad (6)$$

where $\mathbb{1}$ is the indicator function, $\text{Im}(\varphi)$ is the image of the mapping φ . As for character classification, we exploit the

CTC loss to address the length inconsistency issue between the GT text scripts and predictions:

$$\mathcal{L}_{text}^{(k)} = \mathbb{1}_{\{k \in \text{Im}(\varphi)\}} \text{CTC}(t^{(\varphi^{-1}(k))}, \hat{t}_n^{(k)}). \quad (7)$$

In addition, L1 distance loss is used for supervising points coordinates on the center curve and the boundaries (*i.e.*, the top and bottom curves):

$$\mathcal{L}_{coord}^{(k)} = \mathbb{1}_{\{k \in \text{Im}(\varphi)\}} \sum_{n=0}^{N-1} \|p_n^{(\varphi^{-1}(k))} - \hat{p}_n^{(k)}\|, \quad (8)$$

$$\mathcal{L}_{bd}^{(k)} = \mathbb{1}_{\{k \in \text{Im}(\varphi)\}} \sum_{n=0}^{N-1} \left(\|top_n^{(\varphi^{-1}(k))} - \hat{top}_n^{(k)}\| + \|bot_n^{(\varphi^{-1}(k))} - \hat{bot}_n^{(k)}\| \right). \quad (9)$$

The loss function for the decoder consists of the four aforementioned losses:

$$\mathcal{L}_{dec} = \sum_k \left(\lambda_{cls} \mathcal{L}_{cls}^{(k)} + \lambda_{text} \mathcal{L}_{text}^{(k)} + \lambda_{coord} \mathcal{L}_{coord}^{(k)} + \lambda_{bd} \mathcal{L}_{bd}^{(k)} \right), \quad (10)$$

where the hyper-parameters λ_{cls} , λ_{text} , and λ_{coord} are the same as those in Eq. (5). λ_{bd} is the boundary loss weight. In addition, to make the Bezier center curve proposals introduced in Sec. 3.2 more accurate, we resort to adding intermediate supervision on the encoder. As we hope the points sampled on the Bezier center curve proposals are as close to the GT as possible, we calculate the L1 loss for the N uniformly sampled points instead of only the four Bezier control points for each instance. This supervision method has been explored by [46]. The loss function for the encoder is formulated as:

$$\mathcal{L}_{enc} = \sum_i \left(\lambda_{cls} \mathcal{L}_{cls}^{(i)} + \lambda_{coord} \mathcal{L}_{coord}^{(i)} \right), \quad (11)$$

where bipartite matching is also exploited to get one-to-one matching. The overall loss \mathcal{L} is defined as:

$$\mathcal{L} = \mathcal{L}_{dec} + \mathcal{L}_{enc}. \quad (12)$$

TABLE 1 – The setting of linear layers for different scripts.

Linear Layer	Out Channel	Linear Layer	Out Channel
Arabic	73	Bangla	110
Chinese	5,198	Hindi	108
Japanese	2,295	Korean	1,798
Latin	243	Symbols	55

3.6 DeepSolo++

We present DeepSolo++ for multilingual text spotting. Following [17], [18], we explore a multi-head routing scheme for recognizing. Differently, we let a single decoder solo for multilingual text detection, recognition, and script identification, simplifying the structural pipeline (Fig. 1(a) *vs.* Fig. 1(d)). We only adopt a linear layer for character classification of one language (Tab. 1). Besides, we use a simpler training pipeline compared with previous works [17], [18]. Building upon DeepSolo, we additionally design two simple yet effective techniques for multilingual text spotting, *i.e.*, script token modeling and script-aware matching.

Script Token Modeling. Overall, in addition to the point query described in Sec. 3.3, we introduce a script token with explicit point position to gather the global information of each text instance. With the script token, we can conduct

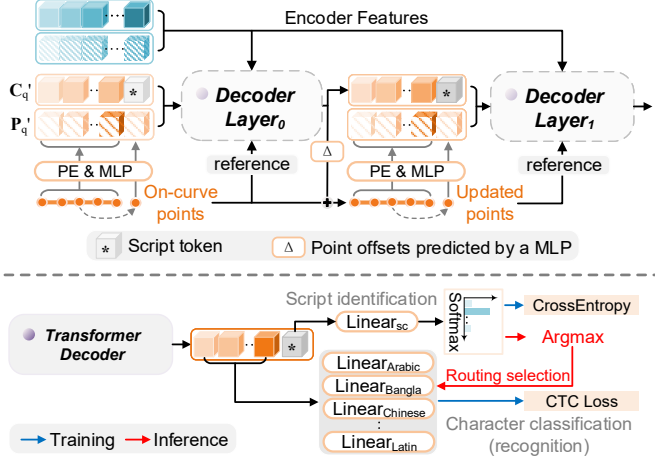


Fig. 3 – The illustration of query modeling (top) in DeepSolo++ and the pipeline of training and inference (bottom). For ease of illustration, only the queries for one text instance are plotted, and only the linear layers for script identification and character classification are shown in the bottom section.

script identification with a linear layer and select the routing recognition result conveniently. The illustration is presented in Fig. 3. Specifically, for script tokens T_{script} , we select the center points of center curve proposals to generate the positional part P_{center} referring to Eq. (2). Then, new content queries C'_q and positional queries P'_q can be obtained by:

$$C'_q = [C_q; T_{script}], P'_q = [P_q; P_{center}]. \quad (13)$$

The composite queries Q'_q of shape $K \times (N + 1) \times 256$ can be achieved by adding C'_q and P'_q . While operating the intra-group self-attention across dimension $N + 1$, there is an attention mask to avoid each script token seeing itself and avoid point queries seeing the script token. Between decoder layers, after updating the points, new center points of center curves are extracted and used for generating the positional part for script tokens. Finally, we conduct script identification based on the script tokens with a linear layer $Linear_{sc}$. Note that only during inference, the output of $Linear_{sc}$ followed by *softmax* and *argmax* operation is used for routing. We simply train $Linear_{sc}$ and the linear layers for character classification in parallel.

Script-aware Matching. In addition to the costs of the instance class, text transcript, and center point coordinates, the script identification cost (*i.e.*, cross-entropy loss) is also involved in calculating the overall cost matrix. The hyper-parameter for balancing script identification cost is set to 1.0. For text transcript cost, each batch may contain instances varying from different scripts, resulting in inconsistent character tables. Therefore, we are not able to directly calculate the text loss using GT and the output of the selected linear layer according to script identification prediction.

To overcome this issue, we design the script-aware matching. The illustration is presented in Fig. 4. To be specific, our target in this period is to get a complete text cost matrix. Firstly, in each batch, we group the GT instances by script types. Next, for each script group, we select the output of the corresponding linear layer to calculate CTC text loss and fill the text cost matrix with the obtained text loss. Since gradients are not calculated during matching, *argmax* can be used to obtain the script identification predictions.

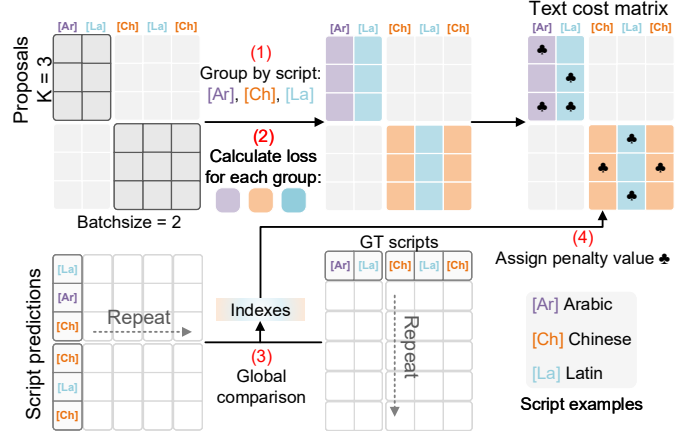


Fig. 4 – The illustration of script-aware matching.

Then, we conduct a global comparison between the script identification prediction and GT. The indexes where the predicted script type is inconsistent with the GT can be obtained. We directly assign a penalty value, which is set to 20 by default, to these positions. Finally, we add text cost matrix and other cost matrices to achieve the overall one, which is used for bipartite matching.

Overall Loss. The script identification loss is additionally included. We also group the GT instances by script type during calculating the text loss. The final text loss is the summation of all script groups. Note that in some datasets, instances do not own their GT script types. It can be obtained by comparing transcripts with the character tables.

4 EXPERIMENTS FOR DEEPSOLO

4.1 Datasets and Evaluation Protocols

We evaluate DeepSolo on **Total-Text** [47], **ICDAR 2015 (IC15)** [48], **SCUT-CTW1500** [49], **ICDAR 2019 ReCTS** [36], and **DAST1500** [50]. **Total-Text** is an arbitrarily-shaped word-level scene text benchmark, which consists of 1,255 training images and 300 testing images. **IC15** contains 1,000 training images and 500 testing images for quadrilateral text. Different from Total-Text and IC15, **SCUT-CTW1500** is a text-line level benchmark for long scene text with arbitrary shapes. There are 1,000 training images and 500 testing images. **ReCTS** is a benchmark for Chinese text on signboards, with 20,000 images used for training and 5,000 images used for evaluation. **DAST1500** is a dense and long text benchmark, which contains 1,038 training images and 500 testing images of commodity packages.

For Total-Text, IC15, and SCUT-CTW1500, we adopt the following additional datasets for pre-training: 1) **Synth150K** [5], a synthetic dataset that contains 94,723 images with multi-oriented texts and 54,327 images with curved texts. 2) **ICDAR 2017 MLT** (MLT17, English only) [39], which is a multilingual scene text dataset. 3) **ICDAR 2013 (IC13)** [51] that contains 229 training images with horizontal text. 4) We also investigate the influence of **TextOCR** [52], which contains 21,778 training and 3,124 validation images.

For ReCTS, following previous works [6], [12], [37], the following datasets are used for pre-training: 1) **SynChinese130K** [6], a synthetic dataset consists of about 130K images. 2) **ICDAR 2019 ArT** [53], which contains 5,603

TABLE 2 – Hyper-parameter study of λ_{text} . ‘E2E’ means the end-to-end spotting results, ‘None’ refers to recognition without any lexicon, and ‘Full’ denotes recognition with a full lexicon that contains all in the test set.

λ_{text}	Detection			E2E	
	P	R	H	None	Full
0.25	94.29	82.07	87.76	76.68	85.76
0.5	93.86	82.11	87.59	78.83	86.15
0.75	94.15	79.27	86.07	78.82	85.71
1.0	93.06	81.71	87.01	77.73	85.61

TABLE 3 – Influence of sharing point embeddings and conducting text matching. The FPS is measured with 1 batch size on one A100 GPU.

Sharing	Matching	Detection			E2E		#Params	FPS
		P	R	H	None	Full		
\times	\checkmark	93.86	82.11	87.59	78.83	86.15	42.5M	17.0
\checkmark	\checkmark	93.60	81.21	86.96	77.58	85.98	41.8M	17.0
\times	\times	92.90	82.11	87.17	77.85	85.20	42.5M	17.0
\checkmark	\times	93.41	81.98	87.32	77.09	85.13	41.8M	17.0

TABLE 4 – The influence of training data.

#Row	External Data	Volume	Detection			E2E	
			P	R	H	None	Full
1	Synth150K	150K	93.86	82.11	87.59	78.83	86.15
2	#1+MLT17+IC13+IC15	160K	93.09	82.11	87.26	79.65	87.00
3	#2+TextOCR	185K	93.19	84.64	88.72	82.54	88.72

training images. 3) **ICDAR 2019 LSVT** [54], a large-scale street view dataset where 30,000 images are used.

We follow the classic evaluation protocols and adopt Precision (P), Recall (R), and H-mean (H) as metrics. H-mean is the primary metric. For the end-to-end text spotting task on ReCTS, Normalized Edit Distance (NED) is adopted to calculate the 1-NED metric [36].

4.2 Implementation Details

The number of heads and sampling points for deformable attention is 8 and 4, respectively. The number of both encoder and decoder layers is 6. The number of proposals K is 100. The number of sampled points N is set to 25 for regular-length datasets, and otherwise 50 for long text benchmark, *i.e.*, SCUT-CTW1500. Our models predict 38 character classes on Total-Text and IC15, 97 classes on CTW1500, and 5,463 classes on ReCTS (the background class is included). AdamW [55] is used as the optimizer. The loss weights λ_{cls} , λ_{coord} , λ_{bd} , and λ_{text} are set to 1.0, 1.0, 0.5, and 0.5, respectively. For focal loss, α is 0.25 and γ is 2.0. The image batch size is 8. Data augmentations include random rotation ($[-45^\circ, +45^\circ]$), random crop, random scale, and color jitter. Since there are no transcript annotations in DAST1500, we abandon the character classification head and set N to 8 for detection. More training details can be found in the supplementary material.

4.3 Ablation Studies

We first conduct ablation experiments on Total-Text, then investigate the influence of the training data and backbone.

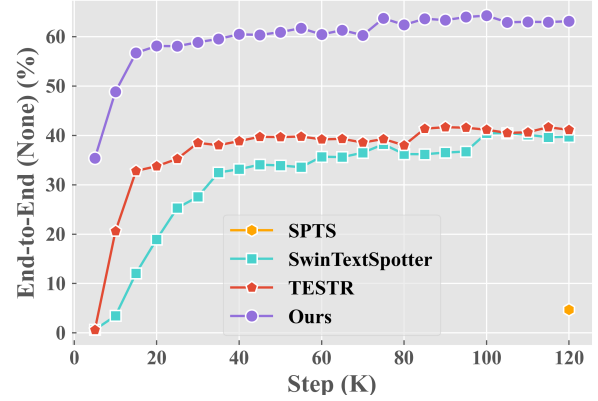


Fig. 5 – Comparison with open-source Transformer-based methods using only Total-Text training set.

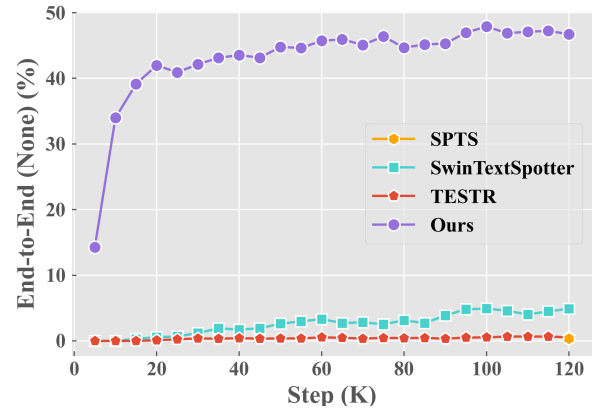


Fig. 6 – Comparison with open-source Transformer-based methods using only SCUT-CTW1500 training set.

TABLE 5 – The influence of different backbones. ‘Mem.’: the peak memory of batching two images on one GPU.

Backbone	Detection			E2E		#Params	Mem. (MB)
	P	R	H	None	Full		
ResNet-50	93.09	82.11	87.26	79.65	87.00	42.5M	17,216
Swin-T	92.77	83.51	87.90	79.66	87.05	43.1M	26,573
ViTAEv2-S	92.57	85.50	88.89	81.79	88.40	33.7M	25,332
ResNet-101	93.20	83.51	88.09	80.12	87.14	61.5M	19,541
Swin-S	93.72	84.24	88.73	81.27	87.75	64.4M	33,974

Text Loss Weight. We study the influence of text loss weight, which has a direct impact on recognition performance. As shown in Tab. 2, our model achieves a better trade-off between detection and end-to-end performance when λ_{text} is set to 0.5. Thus we adopt $\lambda_{\text{text}} = 0.5$ for subsequent experiments.

Sharing Point Embedding. As shown in Tab. 3, when sharing point embeddings for all instances, the results on end-to-end task drop. It indicates that different instances require different point embeddings to encode the instance-specific features.

Text Matching Criterion. To evaluate the effectiveness of the text matching criterion, as shown in Tab. 3, we remove the text matching criterion from Eq. (5). The primary end-to-



Fig. 7 – Qualitative detection results on DAST1500.

TABLE 6 – Detection performance on DAST1500. ‘Ext.’: extra external training data. ‘Res-50’: ResNet-50. ‘+’ denotes the results from [50].

Method	Ext.	P	R	H
SegLink + [56]	✓	66.0	64.7	65.3
CTD+TLOC + [49]	✓	73.8	60.8	66.6
PixelLink + [57]	✓	74.5	75.0	74.7
ICG [50]	✓	79.6	79.2	79.4
ReLaText [58]	✓	89.0	82.9	85.8
MAYOR [59]	✗	87.8	85.5	86.6
DeepSolo (Res-50)	✗	89.1	86.5	87.8

end results decline. It validates the value of conducting text matching, which provides high-quality one-to-one matching according to both position and transcript similarity.

Training Data. We study the influence of different pre-training data in Tab. 4. For the end-to-end spotting task, with only Synth150K as the external pre-training data, our method can achieve 78.83% accuracy without using a lexicon. With additional MLT17, IC13, and IC15 real scene data, the ‘None’ and ‘Full’ scores are improved by 0.82% and 0.85%, respectively. We further show that the performance is improved by a large margin using TextOCR. It demonstrates the value of using real data for pre-training and the scalability of our model on different data. In TextOCR, the average number of text instances per image is higher than in other datasets [52], which can provide more positive signals from the data perspective. Leveraging a real scene dataset with a larger scale and higher average number of instances may be more helpful for training DETR-like scene text detectors and spotters. On the other hand, in the DETR framework, one-to-one matching reduces the training efficiency of positive samples [60], [61]. We speculate that the training efficiency of DeepSolo may also be affected by one-to-one matching. Improving the flaw of one-to-one matching while maintaining a low computational cost is worth further exploration.

We also compare DeepSolo with existing open-source Transformer-based methods [12], [23], [24] by only using the training set of Total-Text. For a fair comparison, we apply the same data augmentation. Since both TESTR and our method are based on Deformable-DETR [34], we set the same configuration for the Transformer modules. ResNet-50 [62] is adopted in all experiments. The image batch size is set to 8, while the actual batch size of SPTS doubles due to batch augmentation. In Fig. 5, our method achieves faster convergence and better performance in the case of limited data volume, showing the superiority of DeepSolo over representative ones in training efficiency.

Making a step further, we compare the training efficiency

TABLE 7 – Detection performance on SCUT-CTW1500. For the detection part, methods in the top section do not adopt DETR-like framework.

Method	Ext.	P	R	H
CRAFT [63]	✓	86.0	81.1	83.5
ContourNet [64]	✗	83.7	84.1	83.9
PAN++ [7]	✓	87.1	81.1	84.0
DRRG [65]	✓	85.9	83.0	84.5
TextFuseNet [66]	✓	85.8	85.0	85.4
TextBPN++ (Res-50-DCN) [67]	✓	88.3	84.7	86.5
FCENet (Res-50-DCN) [68]	✗	87.6	83.4	85.5
MAYOR [59]	✓	88.7	83.6	86.1
DBNet++ [69]	✓	87.9	82.8	85.3
I3CL [42]	✓	88.4	84.6	86.5
TPSNet [70]	✓	88.7	86.3	87.5
Tang <i>et al.</i> [71]	✓	88.1	82.4	85.2
TESTR [23]	✓	<u>92.0</u>	82.6	87.1
SwinTS (Swin-T) [12]	✓	—	—	88.0
DPTText-DETR [27]	✓	91.7	<u>86.2</u>	<u>88.8</u>
DeepSolo (Res-50)	✗	89.6	85.8	87.7
DeepSolo (Res-50)	✓	92.5	86.3	89.3

of our method with others on the long text benchmark, *i.e.*, SCUT-CTW1500. We adopt the default recognition structural setting of all methods on SCUT-CTW1500. As shown in Fig. 6, DeepSolo almost presents an emergent ability while using only the 1,000 training images. A direct reason is that the ‘None’ metric is nonlinear [72]. For long text detection and recognition, thanks to our proposed query form which contributes a unified representation, the two tasks are naturally aligned. Compared with TESTR which adopts dual decoders and heterogeneous queries, the results demonstrate the value of our proposed query form, which encodes a more accurate and explicit position prior and facilitates the learning of the single decoder. Consequently, our simpler design effectively mitigates the synergy issue and shows better training efficiency.

Different Backbones. We conduct experiments to investigate the influence of different backbones in Tab. 5. We select ResNet, Swin Transformer [21], and ViTAEv2 [74] for comparison. All the models are pre-trained with the mixture data as listed in Row #2 of Tab. 4. Compared with ResNet-50, ViTAEv2-S outperforms it by a large margin on the end-to-end spotting task, *i.e.*, 2.14 % on ‘None’ setting. Compared with ResNet-101, Swin-S achieves a gain of 1.15% on ‘None’ setting. We conjecture that the domain gap between large-scale synthetic data and small-scale real data might impact the performance of different backbones. It deserves further exploration to carefully tune the training configuration and study the training paradigm for text spotting.

TABLE 8 – Performance on Total-Text. ‘*’: character-level annotations are used. ‘**’ has the same meaning for other tables.

Method	External Data	Detection			None	Full	FPS (report)	FPS (A100)
		P	R	H				
TextDragon [30]	Synth800K	85.6	75.7	80.3	48.8	74.8	—	—
CharNet [13] *	Synth800K	88.6	81.0	84.6	63.6	—	—	—
TextPerceptron [32]	Synth800K	88.8	81.8	85.2	69.7	78.3	—	—
CRAFTS [16] *	Synth800K+IC13	89.5	85.4	87.4	78.7	—	—	—
Boundary [33]	Synth800K+IC13+IC15	88.9	85.0	87.0	65.0	76.1	—	—
Mask TS v3 [9]	Synth800K+IC13+IC15+SCUT	—	—	—	71.2	78.4	—	—
PGNet [14]	Synth800K+IC15	85.5	<u>86.8</u>	86.1	63.1	—	35.5	—
MANGO [73] *	Synth800K+Synth150K+COCO-Text+MLT19+IC13+IC15	—	—	—	72.9	83.6	4.3	—
PAN++ [7]	Synth800K+COCO-Text+MLT17+IC15	—	—	—	68.6	78.6	21.1	—
ABCNet v2 [6]	Synth150K+MLT17	90.2	84.1	87.0	70.4	78.1	10.0	14.9
TPSNet (Res-50-DCN) [70]	Synth150K+MLT17	90.2	<u>86.8</u>	88.5	76.1	82.3	9.3	—
ABINet++ [37]	Synth150K+MLT17	—	—	—	77.6	84.5	10.6	—
GLASS [10]	Synth800K	90.8	85.5	88.1	79.9	86.2	3.0	—
TESTR [23]	Synth150K+MLT17	<u>93.4</u>	81.4	86.9	73.3	83.9	5.3	12.1
SwinTS (Swin-T) [12]	Synth150K+MLT17+IC13+IC15	—	—	88.0	74.3	84.1	—	2.9
SPTS [24]	Synth150K+MLT17+IC13+IC15	—	—	—	74.2	82.4	—	0.6
TTS (poly) [25]	Synth800K+COCO-Text+IC13+IC15+SCUT	—	—	—	78.2	86.3	—	—
DeepSolo (Res-50)	Synth150K	93.9	82.1	87.6	78.8	86.2	17.0	17.0
DeepSolo (Res-50)	Synth150K+MLT17+IC13+IC15	93.1	82.1	87.3	79.7	87.0	17.0	17.0
DeepSolo (Res-50)	Synth150K+MLT17+IC13+IC15+TextOCR	93.2	84.6	<u>88.7</u>	<u>82.5</u>	<u>88.7</u>	17.0	17.0
DeepSolo (ViTAEv2-S)	Synth150K+MLT17+IC13+IC15+TextOCR	92.9	87.4	90.0	83.6	89.6	10.0	10.0

TABLE 9 – Performance on ICDAR2015. ‘S’, ‘W’ and ‘G’ refer to using strong, weak and generic lexicons, respectively.

Method	External Data	Detection			E2E			Word Spotting		
		P	R	H	S	W	G	S	W	G
TextDragon [30]	Synth800K	<u>92.5</u>	83.8	87.9	82.5	78.3	65.2	86.2	81.6	68.0
CharNet [13] *	Synth800K	91.2	<u>88.3</u>	89.7	80.1	74.5	62.2	—	—	—
TextPerceptron [32]	Synth800K	92.3	82.5	87.1	80.5	76.6	65.1	84.1	79.4	67.9
CRAFTS [16] *	Synth800K+IC13	89.0	85.3	87.1	83.1	82.1	74.9	—	—	—
Boundary [33]	Synth800K+IC13+Total-Text	89.8	87.5	88.6	79.7	75.2	64.1	—	—	—
Mask TS v3 [9]	Synth800K+IC13+Total-Text+SCUT	—	—	—	83.3	78.1	74.2	83.1	79.1	75.1
PGNet [14]	Synth800K+Total-Text	91.8	84.8	88.2	83.3	78.3	63.5	—	—	—
MANGO [73] *	Synth800K+Synth150K+COCO-Text+MLT19+IC13+Total-Text	—	—	—	85.4	80.1	73.9	85.2	81.1	74.6
PAN++ [7]	Synth800K+COCO-Text+MLT17+Total-Text	—	—	—	82.7	78.2	69.2	—	—	—
ABCNet v2 [6]	Synth150K+MLT17	90.4	86.0	88.1	82.7	78.5	73.0	—	—	—
ABINet++ [37]	Synth150K+MLT17	—	—	—	84.1	80.4	75.4	—	—	—
GLASS [10]	Synth800K	86.9	84.5	85.7	84.7	80.1	76.3	86.8	82.5	78.8
TESTR [23]	Synth150K+MLT17+Total-Text	90.3	89.7	<u>90.0</u>	85.2	79.4	73.6	—	—	—
SwinTS (Swin-T) [12]	Synth150K+MLT17+IC13+Total-Text	—	—	—	83.9	77.3	70.5	—	—	—
SPTS [24]	Synth150K+MLT17+IC13+Total-Text	—	—	—	77.5	70.2	65.8	—	—	—
TTS [25]	Synth800K+COCO-Text+IC13+Total-Text+SCUT	—	—	—	85.2	81.7	77.4	85.0	81.5	77.3
DeepSolo (Res-50)	Synth150K+MLT17+IC13+Total-Text	92.8	87.4	<u>90.0</u>	86.8	81.9	76.9	86.3	82.3	77.3
DeepSolo (Res-50)	Synth150K+MLT17+IC13+Total-Text+TextOCR	<u>92.5</u>	87.2	89.8	<u>88.0</u>	<u>83.5</u>	<u>79.1</u>	<u>87.3</u>	<u>83.8</u>	<u>79.5</u>
DeepSolo (ViTAEv2-S)	Synth150K+MLT17+IC13+Total-Text+TextOCR	92.4	87.9	90.1	88.1	83.9	79.5	87.8	84.5	80.0

4.4 Comparison with State-of-the-art Methods

Dense and Long Text. DeepSolo adopts the Bezier center curve to represent scene text, rebuilds the text contour from center to boundary, and conducts explicit point refinement for final detection output. We show that our method effectively handles the detection of dense and long text. **1)** On DAST1500 (Tab. 6), even without pre-training, DeepSolo achieves the best performance, *i.e.*, 87.8% H-mean. Specifically, our method outperforms MAYOR by an absolute 1.2% in terms of H-mean. Compared with ReLaText which adopts a synthetic dataset for pre-training, DeepSolo gets a 2.0% higher H-mean score. Some qualitative detection results are shown in Fig. 7. **2)** On SCUT-CTW1500 (Tab. 7), even without pre-training, DeepSolo achieves 87.7% H-mean, outperforming all methods on the top section. Pre-trained on Synth150K, MLT17, Total-Text, IC13, and IC15, the H-mean is improved by 1.6% to 89.3%.

Results on Total-Text. To evaluate the effectiveness of DeepSolo on scene text with arbitrary shape, we compare our model with state-of-the-art methods in Tab. 8. **1)** Considering the ‘None’ results, with only Synth150K as the external data, our method surpasses previous methods except GLASS. Compared with other Transformer-based methods, DeepSolo significantly outperforms TESTR, SwinTS, and SPTS by 5.5%, 4.5%, and 4.6%, respectively. DeepSolo also outperforms TTS by 0.6% while using far less training data. **2)** With additional MLT17, IC13, and IC15 real data, DeepSolo achieves 79.7% in the ‘None’ setting, which is comparable with the 79.9% performance of GLASS. Note that DeepSolo runs much faster than GLASS and there is no elaborately tailored module for recognition, *e.g.*, the Global to Local Attention Feature Fusion and the external recognizer in GLASS, while we only use a simple linear layer for recognition output. **3)** When using TextOCR, our



Fig. 8 – Visualization of the spotting results, attention on different scale features, and attention of point queries.

TABLE 10 – End-to-end recognition performance on SCUT-CTW1500. ‘len’: the maximum recognition length. ‘†’: measured on one A100 GPU.

Method	None	Full	FPS
TextDragon [30]	39.7	72.4	–
TextPerceptron [32]	57.0	–	–
ABCNet v2 (100 len) [6]	57.5	77.2	10.0
MANGO (25 len) [73]	58.9	78.7	8.4
TPSNet(100 len, Res-50-DCN) [70]	59.7	79.2	–
ABINet++ (100 len) [37]	60.2	80.3	–
SwinTS (Swin-T) [12]	51.8	77.0	–
TESTR (100 len) [23]	56.0	81.5	15.9 †
SPTS (100 len) [24]	63.6	83.8	0.8 †
DeepSolo (25 len, Res-50, Synth150K)	60.1	78.4	20.0 †
DeepSolo (50 len, Res-50, Synth150K)	63.2	80.0	20.0 †
DeepSolo (50 len, Res-50)	64.2	81.4	20.0 †

TABLE 11 – Detection and end-to-end text spotting performance (1-NED) on ReCTS.

Method	Detection			1-NED
	P	R	H	
FOTS [4]	78.3	82.5	80.3	50.8
Mask TS v2 [31]	89.3	88.8	89.0	67.8
AE TextSpotter [75]	92.6	91.0	91.8	71.8
ABCNet v2 [6]	<u>93.6</u>	87.5	90.4	62.7
ABINet++ [37]	92.7	<u>89.2</u>	<u>90.9</u>	<u>76.5</u>
SwinTS (Swin-T) [12]	94.1	87.1	90.4	72.5
DeepSolo (Res-50)	92.6	89.0	90.7	78.3

method achieves very promising spotting performance, *i.e.*, 82.5% and 88.7% at the ‘None’ and ‘Full’ settings. With ViTAEv2-S, the results are further improved by 1.1% and 0.9% in terms of ‘None’ and ‘Full’, respectively.

Results on ICDAR 2015. We conduct experiments on ICDAR 2015 to verify the effectiveness of DeepSolo on multi-oriented scene text, as presented in Tab. 9. The results show that DeepSolo achieves decent performance among all the comparing methods. Specifically, compared with Transformer-based methods using the same training datasets, DeepSolo surpasses SwinTS and SPTS by 6.4% and 11.1% on the E2E setting with the generic lexicon. With TextOCR, DeepSolo (ResNet-50) achieves the best ‘S’, ‘W’, and ‘G’ metrics of 88.0%, 83.5%, and 79.1%.

Results on CTW1500. In Tab. 10, pre-trained on Synth150K, DeepSolo with the maximum recognition length of 25 al-

TABLE 12 – End-to-end recognition performance on RoIC13 without using lexicons.

Method	Rotation 45°			Rotation 60°		
	P	R	H	P	R	H
CharNet [13]	34.2	35.5	33.9	10.3	8.4	9.3
Mask TS v2 [31]	66.4	45.8	54.2	68.2	48.3	56.6
Mask TS v3 [9]	88.5	66.8	76.1	88.5	67.6	76.6
SwinTS (Swin-T) [12]	83.4	72.5	77.6	84.6	<u>72.1</u>	<u>77.9</u>
DeepSolo (Res-50)	82.3	74.9	78.4	82.9	74.9	78.7

TABLE 13 – End-to-end recognition performance on Inverse-Text. ‘#1’, ‘#2’, and ‘#3’ denote the row index in Tab. 4.

Method	None	Full
Mask TS v2 [31]	39.0	43.5
ABCNet [5]	22.2	34.3
ABCNet v2 [6]	34.5	47.4
TESTR [23]	34.2	41.6
SwinTS (Swin-T) [12]	55.4	67.9
SPTS [24]	38.3	46.2
DeepSolo (Res-50, #1)	47.6	53.0
DeepSolo (Res-50, #2)	48.5(+0.9)	53.9(+0.9)
DeepSolo (Res-50, #3)	64.6(+17.0)	71.2(+18.2)
DeepSolo (ViTAEv2-S, #3)	68.8(+21.2)	75.8(+22.8)

ready outperforms most of previous approaches on the ‘None’ metric. We further increase the number of point queries from 25 to 50 for each text instance, achieving an absolute 3.1% improvement on the ‘None’ result, without sacrificing inference speed. Following [24], with MLT17, IC13, IC15, and Total-Text as the external training data, DeepSolo presents 64.2% H-mean without using lexicons, being 0.6% better and 25 times faster than SPTS.

Results on ReCTS. Chinese text owns thousands of character classes and far more complicated font structure than Latin, making Chinese text spotting a more difficult task. Following [6], [12], [37], [75], we evaluate Chinese text spotting performance of DeepSolo on ReCTS. We demonstrate that DeepSolo performs quite well compared with previous works, boosting the 1-NED metric to a new record of 78.3%. It is worth noting that DeepSolo is not equipped with any explicit language modeling scheme but outperforms ABINet++ which leverages powerful language modeling by 1.8% in terms of the 1-NED metric. Compared with SwinTS (Swin-T), DeepSolo (Res-50) achieves 5.8% higher 1-NED



Fig. 9 – Qualitative results on Total-Text, IC15, SCUT-CTW1500, ReCTS, RoIC13, and Inverse-Text. The results on Total-Text and Inverse-Text are from the model with ViTAev2-S backbone. Others are from the model with ResNet-50 backbone.

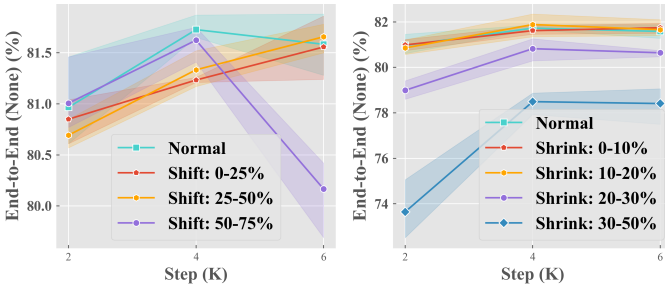


Fig. 10 – Analysis of the sensitivity to different line locations.

performance. It demonstrates the inherent simplicity and remarkable extensibility of DeepSolo in tackling challenging language scenes.

4.5 Spotting Robustness on Rotated Text

We conduct experiments on RoIC13 [9] and Inverse-Text [27] to verify the rotation robustness of DeepSolo. On RoIC13, we fine-tune the pre-trained model (Tab. 4 (#2)) on IC13 using the rotation angles as [9], [12]. As shown in Tab. 12, DeepSolo achieves 78.4% and 78.7% H-mean in Rotation 45° and Rotation 60° settings. Inverse-Text consists of 500 testing images in real scenes with about 40% inverse-like instances. The DeepSolo models reported in Tab. 8 are directly used for evaluation. The stronger rotation augmentation, *i.e.*, using angle chosen from $[-90^\circ, +90^\circ]$ as in SwinTS, is not adopted. Results are shown in Tab. 13. When TextOCR is used, the ‘None’ and ‘Full’ performance are additionally improved by 16.1% and 17.3%, respectively. While replacing ResNet-50 with ViTAev2-S, 4.2% and 4.6% improvements on the two metrics are obtained.

4.6 Visual Analysis

Fig. 8 visualizes the spotting results, the attention on different scale features, and the attention of different point queries. It shows that DeepSolo is capable of correctly recognizing scene texts of large size variance. In the rightmost figure, it is noteworthy that point queries highly attend to the discriminative extremities of characters, which indicates that point queries can effectively encode the character

TABLE 14 – The influence of point position information for script token. ‘Task1’: text detection. ‘Task3’: joint text detection and script identification. ‘Task4’: end-to-end text detection and recognition.

Position	Task1		Task3		Task4		
	H	AP	H	AP	P	R	H
Center	74.8	63.9	73.4	62.3	62.5	42.0	50.3
Start	74.4	63.4	73.0	61.7	61.8	41.3	49.5

TABLE 15 – The influence of text cost penalty in script-aware matching.

Penalty	Task1		Task3		Task4		
	H	AP	H	AP	P	R	H
✓	74.8	63.9	73.4	62.3	62.5	42.0	50.3
✗	75.6	65.5	74.3	63.9	61.0	42.4	50.0

position, scale, and semantic information. More qualitative results are presented in Fig. 9. Interestingly, for the examples marked with red boxes in Total-Text and Inverse-Text, the recognition results are correct even though the detection results are invalid polygons.

4.7 Compatibility to Line Annotations

DeepSolo can adapt to not only polygon annotations but also line annotations, which are much easier to obtain. We conduct experiments on Total-Text with only line annotations. To take advantage of existing full annotations, we first pre-train the model on a mixture of Synth150K, MLT17, IC13, IC15, and TextOCR. Then, we simply exclude the boundary head and fine-tune the model on Total-Text with IC13 and IC15 for 6K steps, using only the text center line annotations. During fine-tuning, the random crop augmentation which needs box information is discarded. We use the evaluation protocol provided by SPTS [24]. To further study the sensitivity to the line location, we randomly shift the center line annotations to the boundary and shrink them to the center point at different levels to simulate annotation errors. Results are plotted in Fig. 10. It can achieve 81.6% end-to-end (‘None’) performance, which is comparable with

TABLE 16 – Text detection results on MLT19 with language-wise performance. The results of CRAFTS are from the official MLT19 website. CRAFTS (paper) denotes the results from their paper [16]. The models in the top section are without a routing structure for multilingual recognition, and the following tables share the same format. ‘#1’ and ‘#3’ denote the row index in Tab. 4, where the pre-trained models are used for initialization.

Method	P	R	H	AP	Arabic	Latin	Chinese	Japanese	Korean	Bangla	Hindi
Single-head TextSpotter [17]	83.8	61.8	71.1	58.8	51.1	73.6	40.4	41.2	56.5	39.7	49.0
CRAFTS [16]	81.4	62.7	70.9	56.6	44.0	72.5	37.2	42.1	54.1	38.5	53.5
CRAFTS (paper) [16]	81.7	70.1	<u>75.5</u>	—	—	—	—	—	—	—	—
Multiplexed TextSpotter [17]	85.5	63.2	72.7	60.5	51.8	73.6	43.9	42.4	57.2	40.3	52.0
DeepSolo++ (Res-50, routing, #1)	<u>85.8</u>	66.2	74.8	<u>63.9</u>	<u>53.1</u>	<u>72.9</u>	<u>49.7</u>	<u>45.1</u>	<u>62.0</u>	<u>42.0</u>	<u>55.7</u>
DeepSolo++ (Res-50, routing, #3)	86.7	<u>68.2</u>	76.3	66.1	54.8	74.9	50.5	45.5	62.7	42.5	56.0

TABLE 17 – Text detection results on MLT17 compared with previous text spotting methods.

Method	P	R	H
FOTS [4]	81.0	57.5	67.3
CharNet [13]	77.1	70.1	73.4
Multiplexed TextSpotter [17]	85.4	62.9	72.4
DeepSolo++ (Res-50, routing, #1)	85.3	65.2	<u>73.9</u>
DeepSolo++ (Res-50, routing, #3)	86.2	<u>67.2</u>	75.6

the fully supervised model, *i.e.*, 82.5%. As shown in Fig. 10, the model is robust to the shift from 0% to 50% and the shrinkage from 0% to 20%. It indicates that the center line should not be too close to the text boundaries and better cover complete character areas.

5 EXPERIMENTS FOR DEEPSOLO++

We validate the effectiveness of DeepSolo++ on ICDAR 2019 MLT [38] and ICDAR 2017 MLT [39]. We evaluate DeepSolo++ on three tasks, *i.e.*, text localization (**MLT19 Task 1**, **MLT17 Task 1**), joint text detection and script identification (**MLT19 Task 3**, **MLT17 Task 3**), and end-to-end text detection and recognition (**MLT19 Task 4**). In Sec. 5.3, we conduct ablation studies on MLT19 for DeepSolo++. Then, we compare DeepSolo++ with previous works on MLT19 and MLT17 in Sec. 5.4.

5.1 Datasets and Evaluation Protocols

ICDAR 2017 MLT (MLT17) [39] contains 7,200 training, 1,800 validation, and 9,000 testing images in 9 languages representing 6 different script types. Multi-oriented scene text instances are annotated with quadrilateral bounding boxes. **ICDAR 2019 MLT (MLT19)** [38] extends MLT17 for the end-to-end text recognition problem and adds a new language (Hindi) to the dataset. MLT19 contains 10,000 training and 10,000 testing images in 10 languages representing 7 different script types. A synthetic dataset (SynthTextMLT) [15] containing 7 scripts is also provided for training.

Following [17], [18], we also adopt the following datasets for pre-training: 1) SynthTextMLT, 2) MLT19, 3) ICDAR 2019 ArT [53], 4) ICDAR 2019 LSVT [36], and 5) ICDAR 2017 RCTW [76], which contains 8,034 Chinese training images. Following the official competitions [38], [39], evaluation protocols include Precision (P), Recall (R), H-mean (H), and Average Precision (AP).

TABLE 18 – Joint text detection and script identification results on MLT19.

Method	P	R	H	AP
Single-head TextSpotter [17]	75.4	57.4	65.2	52.0
CRAFTS [16]	78.5	60.5	68.3	53.8
Multiplexed TextSpotter [17]	81.7	60.3	69.4	56.5
DeepSolo++ (Res-50, routing, #1)	<u>84.3</u>	<u>65.0</u>	<u>73.4</u>	<u>62.3</u>
DeepSolo++ (Res-50, routing, #3)	85.1	66.9	74.9	64.5

TABLE 19 – Joint text detection and script identification results on MLT17.

Method	P	R	H	AP
E2E-MLT [15]	64.6	53.8	58.7	—
CRAFTS [16]	74.5	63.1	68.3	54.6
Multiplexed TextSpotter [17]	81.8	60.3	69.4	56.3
DeepSolo++ (Res-50, routing, #1)	83.7	<u>64.0</u>	<u>72.5</u>	<u>61.1</u>
DeepSolo++ (Res-50, routing, #3)	84.6	65.9	74.1	63.3

5.2 Implementation Details

The number of sampled points N is also set to 25. Other structural settings, such as the number of proposals, are the same as DeepSolo. For training the multilingual text spotter with multi-head routing structure, previous works [17], [18] initialize the weights using the released model of Mask TextSpotter v3 [31] and adopt three-stage training strategy, including training their recognizers individually. For DeepSolo++, we select the model weights in the first and third rows of Tab. 4 for initialization. Then, we pre-train and fine-tune these models on MLT19.

5.3 Ablation Studies

The Positional Source of Script Token. The positional part plays an essential role in modeling the script token. We conduct experiments on the positional source to determine a better choice. We find that using the center point of each center curve is more suitable than using the start point. In Tab. 14, with the center point as the positional source of script token, it achieves 0.4% higher H-mean on both Task 1 and Task 3. The H-mean metric is improved by 0.8% on end-to-end text detection and recognition. We deem that using the start point restricts the script token from attending to more comprehensive information about the whole instance, resulting in worse discrimination.

The Text Cost Penalty in Script-aware Matching. We directly assign a large text penalty value of 20 when the predicted script type is inconsistent with GT. As shown in



Fig. 11 – Text spotting visualization results on ICDAR 2019 MLT.

TABLE 20 – End-to-end recognition results on MLT19.

Method	P	R	H
E2E-MLT [15]	37.4	20.5	26.5
RRPN+CLTDR [77]	38.6	30.1	33.8
Single-head TextSpotter [17]	71.8	27.4	39.7
CRAFTS [16]	65.7	42.7	51.7
CRAFTS (paper) [16]	72.9	48.5	58.2
Multiplexed TextSpotter [17]	68.0	37.3	48.2
Grouped TextSpotter (5 heads) [18]	67.7	37.8	48.5
DeepSolo++ (Res-50, routing, #1)	62.5	42.0	50.3
DeepSolo++ (Res-50, routing, #3)	62.3	43.5	51.2

Tab. 15, this strategy helps to achieve better performance on end-to-end recognition because it implicitly bridges the connection between script identification and recognition, which is desired for end-to-end recognition during inference. But the performance on detection is affected. We speculate that the penalty value is not optimal, thereby affecting the detection part. However, we do not aim to elaborately find the best penalty value in this work. Assigning a progressive penalty value may be more helpful.

5.4 Comparison with State-of-the-art Methods

Text Detection Task. As listed in Tab. 16 and Tab. 17, DeepSolo++ achieves promising detection performance compared with previous spotting methods. On MLT19, DeepSolo++ (Res-50, routing, #1) achieves 74.8% and 63.9% in terms of H-mean and AP metric, surpassing Multiplexed TextSpotter by a large margin. It is noteworthy that DeepSolo++ significantly outperforms previous methods in Chinese, Japanese, and Korean text detection.

Joint Text Detection and Script Identification Task. In Tab. 18 and Tab. 19, without a specific language prediction network, DeepSolo++ shows extraordinary end-to-end script identification ability with a single script token. On MLT19, compared with [17], DeepSolo++ (Res-50, routing, #1) achieves 4.0% higher H-mean and 5.8% higher AP score. DeepSolo++ (Res-50, routing, #3) achieves 5.5% and 8.0% improvement in terms of H-mean and AP, respectively.

End-to-End Recognition Task. As shown in Tab. 20, DeepSolo++ (Res-50, routing, #3) achieves 51.2% H-mean performance, being 2.7% higher than Grouped TextSpotter. However, we notice that there is still a gap between the routing models in the bottom section and the method using a single recognizer, *i.e.*, CRAFTS (paper). On the one hand, CRAFTS

only predicts 4,267 character classes and additionally uses 20,000 images of ReCTS for training [16]. Besides, they use a heavy recognizer which is with 24 Conv layers. On the other hand, the text loss is sparse for all linear layers in our model which are responsible for character classification. Since each batch may not contain all script types, all linear layers cannot be trained together in every step, which might affect the training efficiency.

6 LIMITATION AND DISCUSSION

Although DeepSolo and DeepSolo++ demonstrate promising performance on extensive datasets, there is still some room for improvement. For example, 1) The point order in annotations is in line with the reading order, which implicitly guides the model to learn the text order. However, when the position annotation is not in line with the reading order or the predicted order is incorrect, how to get robust detection [27] and correct recognition is worth further exploration. 2) In DeepSolo++, we model the queries for different languages in a single Transformer decoder. Whether it is necessary to determine a solution to obtain more discriminative features for different languages is unknown and worth further exploration. 3) We do not leverage explicit language modeling. The combination of DETR-based DeepSolo and language modeling may be promising. 4) We simply use a linear layer for character classification. Exploring a more advanced and efficient structure for recognition output is expected. 5) Long-tail recognition issue is still not fixed yet in cutting-edge spotters.

7 CONCLUSION

In this paper, we propose simple yet effective baseline models named DeepSolo and DeepSolo++ for monolingual and multilingual text spotting, taking the merit of a novel explicit point query form that provides a pivotal representation for different tasks. With a single decoder and several simple prediction heads, we present a much simpler method compared with previous text spotters. Our method shows several good properties, including 1) simplicity of structure and training pipeline, 2) efficiency of training and inference, and 3) extensibility of character class, language, and task. Extensive experiments demonstrate that our method has achieved SOTA performance while enjoying some other distinctions, such as the effectiveness on dense and long text, and compatibility to line annotations.

REFERENCES

- [1] X. Chen, L. Jin, Y. Zhu, C. Luo, and T. Wang, "Text recognition in the wild: A survey," *ACM Computing Surveys*, vol. 54, no. 2, pp. 1–35, 2021.
- [2] S. Long, X. He, and C. Yao, "Scene text detection and recognition: The deep learning era," *International Journal of Computer Vision*, vol. 129, no. 1, pp. 161–184, 2021.
- [3] G. N. DeSouza and A. C. Kak, "Vision for mobile robot navigation: A survey," *IEEE Transactions on Pattern Analysis and Machine Intelligence*, vol. 24, no. 2, pp. 237–267, 2002.
- [4] X. Liu, D. Liang, S. Yan, D. Chen, Y. Qiao, and J. Yan, "Fots: Fast oriented text spotting with a unified network," in *CVPR*, 2018, pp. 5676–5685.
- [5] Y. Liu, H. Chen, C. Shen, T. He, L. Jin, and L. Wang, "Abcnet: Real-time scene text spotting with adaptive bezier-curve network," in *CVPR*, 2020, pp. 9809–9818.
- [6] Y. Liu, C. Shen, L. Jin, T. He, P. Chen, C. Liu, and H. Chen, "Abcnet v2: Adaptive bezier-curve network for real-time end-to-end text spotting," *IEEE Transactions on Pattern Analysis and Machine Intelligence*, vol. 44, no. 11, pp. 8048–8064, 2021.
- [7] W. Wang, E. Xie, X. Li, X. Liu, D. Liang, Z. Yang, T. Lu, and C. Shen, "Pan++: Towards efficient and accurate end-to-end spotting of arbitrarily-shaped text," *IEEE Transactions on Pattern Analysis and Machine Intelligence*, vol. 44, no. 9, pp. 5349–5367, 2021.
- [8] P. Lyu, M. Liao, C. Yao, W. Wu, and X. Bai, "Mask textspotter: An end-to-end trainable neural network for spotting text with arbitrary shapes," in *ECCV*, 2018, pp. 67–83.
- [9] M. Liao, G. Pang, J. Huang, T. Hassner, and X. Bai, "Mask textspotter v3: Segmentation proposal network for robust scene text spotting," in *ECCV*, 2020, pp. 706–722.
- [10] R. Ronen, S. Tsiper, O. Anshel, I. Lavi, A. Markovitz, and R. Manmatha, "Glass: global to local attention for scene-text spotting," in *ECCV*, 2022, pp. 249–266.
- [11] H. Zhong, J. Tang, W. Wang, Z. Yang, C. Yao, and T. Lu, "Arts: Eliminating inconsistency between text detection and recognition with auto-rectification text spotter," *arXiv preprint arXiv:2110.10405*, 2021.
- [12] M. Huang, Y. Liu, Z. Peng, C. Liu, D. Lin, S. Zhu, N. Yuan, K. Ding, and L. Jin, "Swintextspotter: Scene text spotting via better synergy between text detection and text recognition," in *CVPR*, 2022, pp. 4593–4603.
- [13] L. Xing, Z. Tian, W. Huang, and M. R. Scott, "Convolutional character networks," in *ICCV*, 2019, pp. 9126–9136.
- [14] P. Wang, C. Zhang, F. Qi, S. Liu, X. Zhang, P. Lyu, J. Han, J. Liu, E. Ding, and G. Shi, "Pgnet: Real-time arbitrarily-shaped text spotting with point gathering network," in *AAAI*, vol. 35, no. 4, 2021, pp. 2782–2790.
- [15] M. Bušta, Y. Patel, and J. Matas, "E2e-mlt-an unconstrained end-to-end method for multi-language scene text," in *ACCV*, 2018, pp. 127–143.
- [16] Y. Baek, S. Shin, J. Baek, S. Park, J. Lee, D. Nam, and H. Lee, "Character region attention for text spotting," in *ECCV*, 2020, pp. 504–521.
- [17] J. Huang, G. Pang, R. Kovvuri, M. Toh, K. J. Liang, P. Krishnan, X. Yin, and T. Hassner, "A multiplexed network for end-to-end, multilingual ocr," in *CVPR*, 2021, pp. 4547–4557.
- [18] J. Huang, K. J. Liang, R. Kovvuri, and T. Hassner, "Task grouping for multilingual text recognition," in *Computer Vision—ECCV 2022 Workshops: Tel Aviv, Israel, October 23–27, 2022, Proceedings, Part IV*, 2023, pp. 297–313.
- [19] A. Vaswani, N. Shazeer, N. Parmar, J. Uszkoreit, L. Jones, A. N. Gomez, L. Kaiser, and I. Polosukhin, "Attention is all you need," in *NeurIPS*, vol. 30, 2017.
- [20] A. Dosovitskiy, L. Beyer, A. Kolesnikov, D. Weissenborn, X. Zhai, T. Unterthiner, M. Dehghani, M. Minderer, G. Heigold, S. Gelly *et al.*, "An image is worth 16x16 words: Transformers for image recognition at scale," in *International Conference on Learning Representations*, 2020.
- [21] Z. Liu, Y. Lin, Y. Cao, H. Hu, Y. Wei, Z. Zhang, S. Lin, and B. Guo, "Swin transformer: Hierarchical vision transformer using shifted windows," in *ICCV*, 2021, pp. 10012–10022.
- [22] Y. Xu, Q. Zhang, J. Zhang, and D. Tao, "Vitate: Vision transformer advanced by exploring intrinsic inductive bias," in *NeurIPS*, vol. 34, 2021, pp. 28522–28535.
- [23] X. Zhang, Y. Su, S. Tripathi, and Z. Tu, "Text spotting transformers," in *CVPR*, 2022, pp. 9519–9528.
- [24] D. Peng, X. Wang, Y. Liu, J. Zhang, M. Huang, S. Lai, J. Li, S. Zhu, D. Lin, C. Shen *et al.*, "Spts: Single-point text spotting," in *ACM MM*, 2022, pp. 4272–4281.
- [25] Y. Kittenplon, I. Lavi, S. Fogel, Y. Bar, R. Manmatha, and P. Perona, "Towards weakly-supervised text spotting using a multi-task transformer," in *CVPR*, 2022, pp. 4604–4613.
- [26] N. Carion, F. Massa, G. Synnaeve, N. Usunier, A. Kirillov, and S. Zagoruyko, "End-to-end object detection with transformers," in *ECCV*, 2020, pp. 213–229.
- [27] M. Ye, J. Zhang, S. Zhao, J. Liu, B. Du, and D. Tao, "Dptext-detr: Towards better scene text detection with dynamic points in transformer," in *AAAI*, 2023.
- [28] K. He, G. Gkioxari, P. Dollár, and R. Girshick, "Mask r-cnn," in *ICCV*, 2017, pp. 2961–2969.
- [29] F. L. Bookstein, "Principal warps: Thin-plate splines and the decomposition of deformations," *IEEE Transactions on Pattern Analysis and Machine Intelligence*, vol. 11, no. 6, pp. 567–585, 1989.
- [30] W. Feng, W. He, F. Yin, X.-Y. Zhang, and C.-L. Liu, "Textdragon: An end-to-end framework for arbitrary shaped text spotting," in *ICCV*, 2019, pp. 9076–9085.
- [31] M. Liao, P. Lyu, M. He, C. Yao, W. Wu, and X. Bai, "Mask textspotter: An end-to-end trainable neural network for spotting text with arbitrary shapes," *IEEE Transactions on Pattern Analysis and Machine Intelligence*, vol. 43, no. 2, pp. 532–548, 2021.
- [32] L. Qiao, S. Tang, Z. Cheng, Y. Xu, Y. Niu, S. Pu, and F. Wu, "Text perceptron: Towards end-to-end arbitrary-shaped text spotting," in *AAAI*, vol. 34, no. 07, 2020, pp. 11899–11907.
- [33] H. Wang, P. Lu, H. Zhang, M. Yang, X. Bai, Y. Xu, M. He, Y. Wang, and W. Liu, "All you need is boundary: Toward arbitrary-shaped text spotting," in *AAAI*, vol. 34, no. 07, 2020, pp. 12160–12167.
- [34] X. Zhu, W. Su, L. Lu, B. Li, X. Wang, and J. Dai, "Deformable detr: Deformable transformers for end-to-end object detection," in *ICLR*, 2021.
- [35] M. Ye, J. Zhang, S. Zhao, J. Liu, T. Liu, B. Du, and D. Tao, "DeepSolo: Let transformer decoder with explicit points solo for text spotting," in *CVPR*, 2023, pp. 19348–19357.
- [36] R. Zhang, Y. Zhou, Q. Jiang, Q. Song, N. Li, K. Zhou, L. Wang, D. Wang, M. Liao, M. Yang *et al.*, "Icdar 2019 robust reading challenge on reading chinese text on signboard," in *ICDAR*. IEEE, 2019, pp. 1577–1581.
- [37] S. Fang, Z. Mao, H. Xie, Y. Wang, C. Yan, and Y. Zhang, "Abinet++: Autonomous, bidirectional and iterative language modeling for scene text spotting," *IEEE Transactions on Pattern Analysis and Machine Intelligence*, pp. 1–18, 2022.
- [38] N. Nayef, Y. Patel, M. Busta, P. N. Chowdhury, D. Karatzas, W. Khlif, J. Matas, U. Pal, J.-C. Burie, C.-I. Liu *et al.*, "Icdar2019 robust reading challenge on multi-lingual scene text detection and recognition—rrc-mlt-2019," in *ICDAR*. IEEE, 2019, pp. 1582–1587.
- [39] N. Nayef, F. Yin, I. Bizid, H. Choi, Y. Feng, D. Karatzas, Z. Luo, U. Pal, C. Rigaud, J. Chazalon *et al.*, "Icdar2017 robust reading challenge on multi-lingual scene text detection and script identification-rrc-mlt," in *ICDAR*, vol. 1, 2017, pp. 1454–1459.
- [40] G. G. Lorentz, *Bernstein polynomials*. American Mathematical Soc., 2013.
- [41] S. Liu, F. Li, H. Zhang, X. Yang, X. Qi, H. Su, J. Zhu, and L. Zhang, "Dab-detr: Dynamic anchor boxes are better queries for detr," in *ICLR*, 2022.
- [42] B. Du, J. Ye, J. Zhang, J. Liu, and D. Tao, "I3cl: Intra-and inter-instance collaborative learning for arbitrary-shaped scene text detection," *International Journal of Computer Vision*, vol. 130, no. 8, pp. 1961–1977, 2022.
- [43] H. W. Kuhn, "The hungarian method for the assignment problem," *Naval research logistics quarterly*, vol. 2, no. 1-2, pp. 83–97, 1955.
- [44] A. Graves, S. Fernández, F. Gomez, and J. Schmidhuber, "Connectionist temporal classification: labelling unsegmented sequence data with recurrent neural networks," in *ICML*, 2006, pp. 369–376.
- [45] T.-Y. Lin, P. Goyal, R. Girshick, K. He, and P. Dollár, "Focal loss for dense object detection," in *ICCV*, 2017, pp. 2980–2988.
- [46] Z. Feng, S. Guo, X. Tan, K. Xu, M. Wang, and L. Ma, "Rethinking efficient lane detection via curve modeling," in *CVPR*, 2022, pp. 17062–17070.
- [47] C.-K. Ch'ng, C. S. Chan, and C.-L. Liu, "Total-text: toward orientation robustness in scene text detection," *IJDAR*, vol. 23, no. 1, pp. 31–52, 2020.
- [48] D. Karatzas, L. Gomez-Bigorda, A. Nicolaou, S. Ghosh, A. Bagdanov, M. Iwamura, J. Matas, L. Neumann, V. R. Chandrasekhar,

- S. Lu *et al.*, "Icdar 2015 competition on robust reading," in *ICDAR*, 2015, pp. 1156–1160.
- [49] Y. Liu, L. Jin, S. Zhang, C. Luo, and S. Zhang, "Curved scene text detection via transverse and longitudinal sequence connection," *Pattern Recognition*, vol. 90, pp. 337–345, 2019.
- [50] J. Tang, Z. Yang, Y. Wang, Q. Zheng, Y. Xu, and X. Bai, "Seglink++: Detecting dense and arbitrary-shaped scene text by instance-aware component grouping," *Pattern recognition*, vol. 96, p. 106954, 2019.
- [51] D. Karatzas, F. Shafait, S. Uchida, M. Iwamura, L. G. i Bigorda, S. R. Mestre, J. Mas, D. F. Mota, J. A. Almazan, and L. P. De Las Heras, "Icdar 2013 robust reading competition," in *ICDAR*, 2013, pp. 1484–1493.
- [52] A. Singh, G. Pang, M. Toh, J. Huang, W. Galuba, and T. Hassner, "Textocr: Towards large-scale end-to-end reasoning for arbitrary-shaped scene text," in *CVPR*, 2021, pp. 8802–8812.
- [53] C. K. Chng, Y. Liu, Y. Sun, C. C. Ng, C. Luo, Z. Ni, C. Fang, S. Zhang, J. Han, E. Ding *et al.*, "Icdar2019 robust reading challenge on arbitrary-shaped text-rrc-art," in *ICDAR*. IEEE, 2019, pp. 1571–1576.
- [54] Y. Sun, Z. Ni, C.-K. Chng, Y. Liu, C. Luo, C. C. Ng, J. Han, E. Ding, J. Liu, D. Karatzas *et al.*, "Icdar 2019 competition on large-scale street view text with partial labeling-rrc-lsvt," in *ICDAR*. IEEE, 2019, pp. 1557–1562.
- [55] I. Loshchilov and F. Hutter, "Decoupled weight decay regularization," in *ICLR*, 2019.
- [56] B. Shi, X. Bai, and S. Belongie, "Detecting oriented text in natural images by linking segments," in *CVPR*, 2017, pp. 2550–2558.
- [57] D. Deng, H. Liu, X. Li, and D. Cai, "Pixellink: Detecting scene text via instance segmentation," in *AAAI*, vol. 32, no. 1, 2018.
- [58] C. Ma, L. Sun, Z. Zhong, and Q. Huo, "Relatext: exploiting visual relationships for arbitrary-shaped scene text detection with graph convolutional networks," *Pattern Recognition*, vol. 111, p. 107684, 2021.
- [59] X. Qin, Y. Zhou, Y. Guo, D. Wu, Z. Tian, N. Jiang, H. Wang, and W. Wang, "Mask is all you need: Rethinking mask r-cnn for dense and arbitrary-shaped scene text detection," in *ACM MM*, 2021, pp. 414–423.
- [60] W. Wang, J. Zhang, Y. Cao, Y. Shen, and D. Tao, "Towards data-efficient detection transformers," in *ECCV*. Springer, 2022, pp. 88–105.
- [61] D. Jia, Y. Yuan, H. He, X. Wu, H. Yu, W. Lin, L. Sun, C. Zhang, and H. Hu, "Detrs with hybrid matching," in *CVPR*, 2023, pp. 19702–19712.
- [62] K. He, X. Zhang, S. Ren, and J. Sun, "Deep residual learning for image recognition," in *CVPR*, 2016, pp. 770–778.
- [63] Y. Baek, B. Lee, D. Han, S. Yun, and H. Lee, "Character region awareness for text detection," in *CVPR*, 2019, pp. 9365–9374.
- [64] Y. Wang, H. Xie, Z.-J. Zha, M. Xing, Z. Fu, and Y. Zhang, "Contournet: Taking a further step toward accurate arbitrary-shaped scene text detection," in *CVPR*, 2020, pp. 11753–11762.
- [65] S.-X. Zhang, X. Zhu, J.-B. Hou, C. Liu, C. Yang, H. Wang, and X.-C. Yin, "Deep relational reasoning graph network for arbitrary shape text detection," in *CVPR*, 2020, pp. 9699–9708.
- [66] J. Ye, Z. Chen, J. Liu, and B. Du, "Textfusenet: Scene text detection with richer fused features," in *IJCAI*, vol. 20, 2020, pp. 516–522.
- [67] S.-X. Zhang, X. Zhu, C. Yang, and X.-C. Yin, "Arbitrary shape text detection via boundary transformer," *arXiv preprint arXiv:2205.05320*, 2022.
- [68] Y. Zhu, J. Chen, L. Liang, Z. Kuang, L. Jin, and W. Zhang, "Fourier contour embedding for arbitrary-shaped text detection," in *CVPR*, 2021, pp. 3123–3131.
- [69] M. Liao, Z. Zou, Z. Wan, C. Yao, and X. Bai, "Real-time scene text detection with differentiable binarization and adaptive scale fusion," *IEEE Transactions on Pattern Analysis and Machine Intelligence*, vol. 45, no. 1, pp. 919–931, 2022.
- [70] W. Wang, Y. Zhou, J. Lv, D. Wu, G. Zhao, N. Jiang, and W. Wang, "Tpsnet: Reverse thinking of thin plate splines for arbitrary shape scene text representation," in *ACM MM*, 2022, pp. 5014–5025.
- [71] J. Tang, W. Zhang, H. Liu, M. Yang, B. Jiang, G. Hu, and X. Bai, "Few could be better than all: Feature sampling and grouping for scene text detection," in *CVPR*, 2022, pp. 4563–4572.
- [72] R. Schaeffer, B. Miranda, and S. Koyejo, "Are emergent abilities of large language models a mirage?" *arXiv preprint arXiv:2304.15004*, 2023.
- [73] L. Qiao, Y. Chen, Z. Cheng, Y. Xu, Y. Niu, S. Pu, and F. Wu, "Mango: A mask attention guided one-stage scene text spotter," in *AAAI*, vol. 35, no. 3, 2021, pp. 2467–2476.
- [74] Q. Zhang, Y. Xu, J. Zhang, and D. Tao, "Vitaev2: Vision transformer advanced by exploring inductive bias for image recognition and beyond," *International Journal of Computer Vision*, pp. 1–22, 2023.
- [75] W. Wang, X. Liu, X. Ji, E. Xie, D. Liang, Z. Yang, T. Lu, C. Shen, and P. Luo, "Ae textspotter: Learning visual and linguistic representation for ambiguous text spotting," in *ECCV*, 2020, pp. 457–473.
- [76] B. Shi, C. Yao, M. Liao, M. Yang, P. Xu, L. Cui, S. Belongie, S. Lu, and X. Bai, "Icdar2017 competition on reading chinese text in the wild (rctw-17)," in *ICDAR*, vol. 1. IEEE, 2017, pp. 1429–1434.
- [77] J. Ma, W. Shao, H. Ye, L. Wang, H. Wang, Y. Zheng, and X. Xue, "Arbitrary-oriented scene text detection via rotation proposals," *IEEE Transactions on Multimedia*, vol. 20, no. 11, pp. 3111–3122, 2018.

DeepSolo++: Let Transformer Decoder with Explicit Points Solo for Text Spotting

— Supplemental Material —

1 DETAILS OF DEEPSOLO WITH RESNET

The training details of DeepSolo with ResNet [3] (ImageNet pre-trained weights from TORCHVISION) are listed in Tab. 1 with corresponding training data, learning rate, and iterations.

In Fig. 5 and Fig. 6 of the main paper, *i.e.*, only the Total-Text or CTW1500 training set is utilized, the training schedule of DeepSolo is related to Row #9 and Row #10, respectively. For SPTS [4], we only plot the final performance since SPTS needs more data and a longer training schedule to achieve ideal performance.

The training setting of DeepSolo with line labels is provided in Row #12. During fine-tuning, the line annotations are used and stronger rotation augmentation (angle randomly chosen from $[-90^\circ, +90^\circ]$) is adopted.

2 DETAILS OF DEEPSOLO WITH SWIN TRANSFORMER

In Tab. 5 of the main paper, with Swin Transformer [5], we pre-train the model for 375K iterations and fine-tune it on Total-Text for 10K iterations. No part of the backbone is frozen. During pre-training, the initial learning rate for the backbone is $1e^{-4}$. The drop path rate of Swin-T and Swin-S is set to 0.2 and 0.3, respectively. During fine-tuning, we set the learning rate for the backbone to $1e^{-5}$, and the drop path rate to 0.2 and 0.3 for Swin-T and Swin-S. Other training schedules are the same as Row #2 in Tab. 1.

3 DETAILS OF DEEPSOLO WITH VITAE

With ViTAEv2-S [6], the drop path rate is set to 0.3 for pre-training and 0.2 for fine-tuning. Other training schedules are the same as Swin Transformer backbone.

4 MORE VISUALIZATIONS

4.1 Visualizations of Line Annotations

In Sec. 4.7 of the main paper, we study the model sensitivity to different line locations. We provide a group of visualizations in Fig. 1 to intuitively show the noisy line locations.



Fig. 1 – The illustration of line labels at different noisy levels.

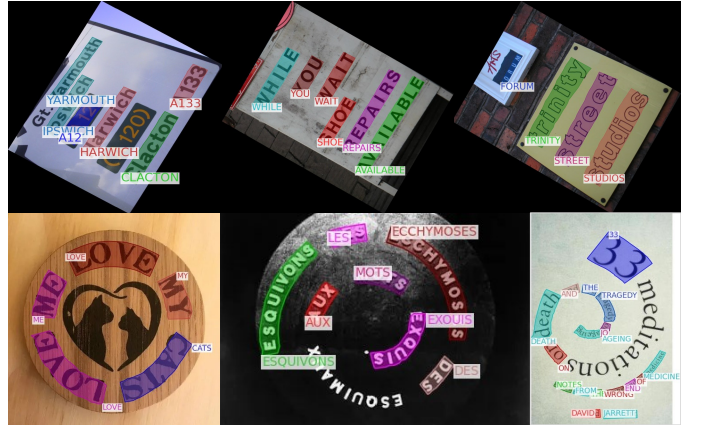


Fig. 2 – Spotting visualizations on RoIC13 (the first row, ResNet-50 backbone) and Inverse-Text (the bottom row, ViTAEv2-S backbone).

4.2 Visualizations on RoIC13 and Inverse-Text

More qualitative results on RoIC13 and Inverse-Text are provided in Fig. 2. In the bottom row, some upside-down instances are not detected, which is also a main issue while spotting inverse-like instances. Correctly detecting and recognizing inverse-like text requires more discriminative features.

REFERENCES

- [1] T.-Y. Lin, P. Goyal, R. Girshick, K. He, and P. Dollár, “Focal loss for dense object detection,” in ICCV, 2017, pp. 2980–2988.

TABLE 1 – Training details of DeepSolo with ResNet. ‘Step’ denotes the iteration step where the learning rate is divided by 10.

#Row	Backbone	Pre-training				Fine-tuning				Where in the Main Paper
		Training Data	lr (Backbone)	Iterations	Step	Training Data	lr (Backbone)	Iterations	Step	
1	ResNet-50	Synth150K+Total-Text	$1e^{-4}$ ($1e^{-5}$)	350K	300K	Total-Text	$1e^{-5}$ ($1e^{-6}$)	10K	–	Tab. 2, 3, 4, 8
2		Synth150K+Total-Text+MLT17+IC13+IC15	$1e^{-4}$ ($1e^{-5}$)	375K	320K	Total-Text	$1e^{-5}$ ($1e^{-6}$)	10K	–	Tab. 4, 5, 8
3		Synth150K+Total-Text+MLT17+IC13+IC15+TextOCR	$1e^{-4}$ ($1e^{-5}$)	435K	375K	Total-Text	$1e^{-5}$ ($1e^{-6}$)	2K	–	Tab. 4, 8
4		Synth150K+Total-Text+MLT17+IC13+IC15	$1e^{-4}$ ($1e^{-5}$)	375K	320K	IC15	$1e^{-5}$ ($1e^{-6}$)	3K	–	Tab. 9
5		Synth150K+Total-Text+MLT17+IC13+IC15+TextOCR	$1e^{-4}$ ($1e^{-5}$)	435K	375K	IC15	$1e^{-5}$ ($1e^{-6}$)	1K	–	Tab. 9
6		Synth150K+Total-Text+MLT17+IC13+IC15	$1e^{-4}$ ($1e^{-5}$)	375K	320K	CTW1500	$5e^{-5}$ ($5e^{-6}$)	12K	8K	Tab. 7, 10
7		SynChinese130K+ArT+LSVT+ReCTS	$1e^{-4}$ ($1e^{-5}$)	400K	300K	ReCTS	$1e^{-5}$ ($1e^{-6}$)	30K	20K	Tab. 11
8		Synth150K+Total-Text+MLT17+IC13+IC15	$1e^{-4}$ ($1e^{-5}$)	375K	320K	IC13	$1e^{-5}$ ($1e^{-6}$)	1K	–	Tab. 12
9		Total-Text	$1e^{-4}$ ($1e^{-5}$)	120K	80K	–	–	–	–	Fig. 5
10		CTW1500	$1e^{-4}$ ($1e^{-5}$)	120K	90K	–	–	–	–	Fig. 6, Tab. 7
11		DAST1500	$1e^{-4}$ ($1e^{-5}$)	80K	70K, 78K	–	–	–	–	Tab. 6
12		Synth150K+MLT17+IC13+IC15+TextOCR	$1e^{-4}$ ($1e^{-5}$)	435K	375K	Total-Text+IC13+IC15	$2e^{-5}$ ($2e^{-6}$)	6K	–	Fig. 10
13		SynthTextMLT+MLT19+ArT+LSVT+RCTW	$1e^{-4}$ ($1e^{-5}$)	600K	450K	MLT19	$1e^{-5}$ ($1e^{-6}$)	50K	–	Tab. 14-20
14	ResNet-101	Synth150K+Total-Text+MLT17+IC13+IC15	$1e^{-4}$ ($1e^{-5}$)	375K	320K	Total-Text	$1e^{-5}$ ($1e^{-6}$)	10K	–	Tab. 5

TABLE 2 – Lookup table for key notations in the paper.

Notation	Description
K	number of Bezier center curve proposals
N	number of sampled points on each Bezier center curve
MLP	multi-layer perceptron
PE	positional encoding
\hat{p}	2D normalized coordinates
Δp	offsets predicted by an MLP
BP	Bezier center curve proposals where each is determined by four control points
\hat{BP}	top- K curve proposals selected from BP
$Coords$	normalized point coordinates of shape $K \times N \times 2$, sampled from \hat{BP}
σ	sigmoid function
σ^{-1}	inverse sigmoid function
\mathbf{P}_q	positional queries
\mathbf{C}_q	content queries
\mathbf{Q}_q	composite queries achieved by: $\mathbf{P}_q + \mathbf{C}_q$
λ_{cls}	loss weight for instance classification
λ_{text}	loss weight for text recognition
λ_{coord}	loss weight for point coordinates on center curve
λ_{bd}	loss weight for point coordinates on instance boundary
\mathcal{L}_{cls}	instance classification loss (text or not text), derived from focal loss [1]
\mathcal{L}_{text}	text recognition loss (CTC loss [2])
\mathcal{L}_{coord}	L1 distance loss for point coordinates on center curve
\mathcal{L}_{bd}	L1 distance loss for point coordinates on instance boundary
\mathcal{L}_{dec}	loss function for decoder part, consisting of \mathcal{L}_{cls} , \mathcal{L}_{text} , \mathcal{L}_{coord} , and \mathcal{L}_{bd}
\mathcal{L}_{enc}	loss function for encoder part, consisting of \mathcal{L}_{cls} and \mathcal{L}_{coord}
\mathcal{L}	overall loss achieved by: $\mathcal{L}_{dec} + \mathcal{L}_{enc}$
T_{script}	script tokens
\mathbf{P}'_q	positional queries combining \mathbf{P}_q and the center point positional queries in \mathbf{P}_q
\mathbf{C}'_q	content queries combining \mathbf{C}_q and T_{script}
\mathbf{Q}'_q	composite queries achieved by: $\mathbf{P}'_q + \mathbf{C}'_q$

- [2] A. Graves, S. Fernández, F. Gomez, and J. Schmidhuber, “Connectionist temporal classification: labelling unsegmented sequence data with recurrent neural networks,” in *ICML*, 2006, pp. 369–376.
- [3] K. He, X. Zhang, S. Ren, and J. Sun, “Deep residual learning for image recognition,” in *CVPR*, 2016, pp. 770–778.
- [4] D. Peng, X. Wang, Y. Liu, J. Zhang, M. Huang, S. Lai, J. Li, S. Zhu, D. Lin, C. Shen *et al.*, “Spts: Single-point text spotting,” in *ACM MM*, 2022, pp. 4272–4281.
- [5] Z. Liu, Y. Lin, Y. Cao, H. Hu, Y. Wei, Z. Zhang, S. Lin, and B. Guo, “Swin transformer: Hierarchical vision transformer using shifted windows,” in *ICCV*, 2021, pp. 10012–10022.
- [6] Q. Zhang, Y. Xu, J. Zhang, and D. Tao, “Vitaev2: Vision transformer advanced by exploring inductive bias for image recognition and beyond,” *International Journal of Computer Vision*, pp. 1–22, 2023.